RESEARCH ARTICLE
10.1002/2013JC009718

Key Point:
- The present model is able to recover near-bed information in field measurements

Correspondence to:
R. Mathis,
romain.mathis@univ-lille1.fr

Citation:
Mathis, R., I. Marusic, O. Cabrit, N. L. Jones, and G. N. Ivey (2014), Modeling bed shear-stress fluctuations in a shallow tidal channel, *J. Geophys. Res. Oceans*, *119*, doi:10.1002/2013JC009718.

Modeling bed shear-stress fluctuations in a shallow tidal channel

R. Mathis[1], I. Marusic[2], O. Cabrit[2], N. L. Jones[3], and G. N. Ivey[3]

[1]Laboratoire de Mécanique de Lille, CNRS UMR 8107, Université Lille Nord de France, Villeneuve d'Ascq, France, [2]Department of Mechanical Engineering, University of Melbourne, Melbourne, Victoria, Australia, [3]School of Environmental Systems Engineering and UWA Oceans Institute, University of Western Australia, Crawley, Western Australia, Australia

Abstract Recently, Mathis et al. (2013) developed a model for predicting the instantaneous fluctuations of the wall shear-stress in turbulent boundary layers. This model is based on an inner-outer scale interaction mechanism, incorporating superposition, and amplitude-modulation effects, and the only input required for the model is a time series measurement of the streamwise velocity signal taken in the logarithmic region of the flow. The present study applies this new approach for the first time to environmental flows, for which the near-bed information is typically inaccessible. The data used here are acoustic Doppler velocimeter time series measurements from a shallow tidal channel (Suisun Slough in North San Francisco Bay). We first extract segments of data sharing properties with canonical turbulent boundary layers. The wall (bed) shear-stress model is then applied to these selected data. Statistical and spectral analysis demonstrates that the field data predictions are consistent with laboratory and DNS results. The model is also applied to the whole available data set to demonstrate, even for situations far from the canonical boundary layer case, its ability to preserve the overall Reynolds number trend. The predicted instantaneous bed stress is highly skewed and amplitude modulated with the variations in the large-scale streamwise velocity. Finally, the model is compared to conventional methods employed to predict the bed shear-stress. A large disparity is observed, but the present model is the only one able to predict both the correct spectral content and the probability density function.

1. Introduction

In wall-bounded turbulent flows the wall shear-stress τ_w constitutes a key parameter for accurate prediction of the flow behavior. Over the years, many studies have been devoted toward understanding and modeling the Reynolds number dependency of the time-averaged streamwise component, $\bar{\tau}_w$, which is used in boundary layer inner-scaling via the friction velocity $U_\tau = \sqrt{\bar{\tau}_w/\rho}$, where ρ is the fluid density [see, e.g., *Schlichting and Gersten*, 2000; *Monkewitz et al.*, 2007, among others]. However, little is known about the fluctuating component, τ_w', which can be responsible for extreme and destructive events, such as wind gusts in atmospheric flows or scouring and mechanical damage on an aircraft [see *Örlü and Schlatter*, 2011, Figure 3]. In environmental flows, the wall or bed shear-stress is of great ecological importance where it is linked to erosion, bed formation, sediment, and nutrient transportation, etc. [e.g., *Grant and Madsen*, 1986; *Rowiński et al.*, 2005; *Grant and Marusic*, 2012; *Simpson and Sharples*, 2012]. For example, following *Shields* [1936], knowledge of sediment properties has traditionally been combined with estimates of the time-averaged bed shear-stress to predict the incipient motion of sediment particles.

Prediction of the bed shear-stress fluctuations has a wide range of applications, from riverine flow streams to atmospheric surface layers. For example, bed shear-stress fluctuations influence turbulent mixing coastal ocean bottom boundaries, pollution emission, and alteration of the water cycle in the atmosphere. Specifically, recent work [e.g., *Diplas et al.*, 2008] has suggested that rather than simply the time-averaged shear-stress, the instantaneous turbulent forces and their duration are important in initiating the motion of particles. Unfortunately, the instantaneous bed shear-stress is largely inaccessible in field measurements, which prompts the need for predictive models to reconstruct the missing information. In this paper, we test and apply a new approach [*Mathis et al.*, 2013] to predict the instantaneous bed shear-stress for an environmental flow, where the near-bed information is typically inaccessible. Here the fluctuating component is defined as $\tau_w'(\mathbf{x}, t) = \tau_w(\mathbf{x}, t) - \bar{\tau}_w(\mathbf{x})$, where $\tau_w(\mathbf{x}, t)$ and $\bar{\tau}_w(\mathbf{x})$ are the total and mean values of the bed shear-stress,

respectively, and $\mathbf{x}=(x,y)$ denotes the position vector in the plane of the wall. The coordinates x, y, and z refer to the streamwise, spanwise, and bed-normal directions. The respective fluctuating velocity components are denoted by u', v', and w', and over-bars indicate time-averaged values (e.g., $u=\bar{u}+u'$). The superscript "+" is used to denote nondimensional viscous scaling of length $z^+=zU_\tau/\nu$ (also read as wall unit) and velocities $u^+=u/U_\tau$, where ν is the kinematic viscosity of the fluid (taken as $\nu=1.05\times10^{-6}$ m^2/s in this study).

Recently, *Mathis et al*. [2013] (hereafter denoted M13) proposed a novel predictive model able to reconstruct the fluctuating wall shear-stress based on single point large-scale time series measurements taken away from the wall, ideally in the log-layer. In this paper, "large-scale" denotes extended periods of positive or negative fluctuations observed in time series measurements, characterized by low-frequency (or long-wavelength) events. The model is based on extensive empirical observations, both experimental and numerical, that have clearly established the existence of a strong interaction between the near-wall region and motions in the outer region. The Reynolds number effects are closely related to the increasingly energetic content of the large-scale structures associated with the log-layer [*Kim and Adrian*, 1999; *del Álamo and Jiménez*, 2003; *Hutchins and Marusic*, 2007a, among others], through superposition and modulation effects [*Bandyopadhyay and Hussain*, 1984; *Grinvald and Nikora*, 1988; *Hutchins and Marusic*, 2007b; *Mathis et al*., 2009, 2011]. We note that the Reynolds number effects discussed here correspond to a rise of the turbulent averaged quantities and wall shear-stress variance as the Reynolds number increases. The wall shear-stress model was originally derived from the streamwise velocity model developed by *Marusic et al*. [2010] and *Mathis et al*. [2011], where an algebraic relationship between the streamwise velocity component and the wall shear-stress is known, and is of the form:

$$\tau_{wp}^{\prime+}(t^+)=\tau_w^{\prime*}(t^+)\left[1+\alpha u_{OL}^{\prime+}(t^+)\right]+\alpha u_{OL}^{\prime+}(t^+), \tag{1}$$

where $\tau_{wp}^{\prime+}$ is the predicted time series normalized by wall variables, $\tau_{wp}^{\prime+}=\tau_{wp}^{\prime}/(\rho U_\tau^2)$ and $t^+=tU_\tau^2/\nu$. The time series $\tau_w^{\prime*}$, which is normalized in wall units, represents the statistically "universal" wall shear-stress signal free of any Reynolds number effects. Indeed, as proposed by M13, the time series $\tau_w^{\prime*}$ and the universal (see below) parameter α can be determined from a *once-off* calibration experiment at an arbitrarily chosen Reynolds number (above a minimum value, say $Re_\tau=4000$, to ensure enough separation between the inner and outer scales). The only user input required is the large-scale streamwise velocity signal, $u_{OL}^{\prime+}$, ideally taken at the logarithmic center of the log-layer, $z_O^+=\sqrt{15Re_\tau}$, where $Re_\tau=U_\tau\delta/\nu$ is the friction Reynolds number and δ the boundary layer thickness [see *Mathis et al*., 2009, 2011, for further details about the choice of z_O^+]. The model consists of two parts. The first part in equation (1), $\tau_w^{\prime*}(t^+)\left[1+\alpha u_{OL}^{\prime+}(t^+)\right]$, models the amplitude modulation of the small-scale wall shear-stress fluctuations, $\tau_w^{\prime*}$, by the large-scale motions within the log-layer, $u_{OL}^{\prime+}$. The second term, $\alpha u_{OL}^{\prime+}$, models the superposition effect of the large-scale motions felt at the wall. The underlying idea is that the near-wall small-scale motions are universal (i.e., they do not change with Reynolds number), and therefore are only influenced by large-scale events (the intensity of this influence increasing with Reynolds number). Therefore, the Reynolds number effects are entirely confined to the input signal, $u_{OL}^{\prime+}$. The practical motivations behind the development of the M13 model are twofold. First, the difficulty of measuring the instantaneous friction velocity in the turbulent boundary layer, particularly at high Reynolds numbers, indicates the need to develop alternative methods to recover information in the vicinity of the wall. Second, from a numerical point of view, the M13 model constitutes a possible improvement on the existing wall-models employed to save computational resources in high Reynolds number simulations.

The purpose of the present study is to assess the applicability of M13 model to environmental flows, where effects such as bed roughness and/or density stratification may be important. The M13 model was initially developed and calibrated for the flat-plate smooth-wall turbulent boundary layer, and therefore its applicability in environmental flows may not be straightforward. We use water column measurements from a shallow tidal channel to predict the instantaneous bed shear-stress. Results, including statistical properties and spectral content, are analyzed and compared with canonical flat-plate smooth-wall turbulent boundary layer data available in the literature, and with previous predictions made with high-fidelity laboratory measurements. It should be emphasized that the objective of this work is not to validate the M13 model against

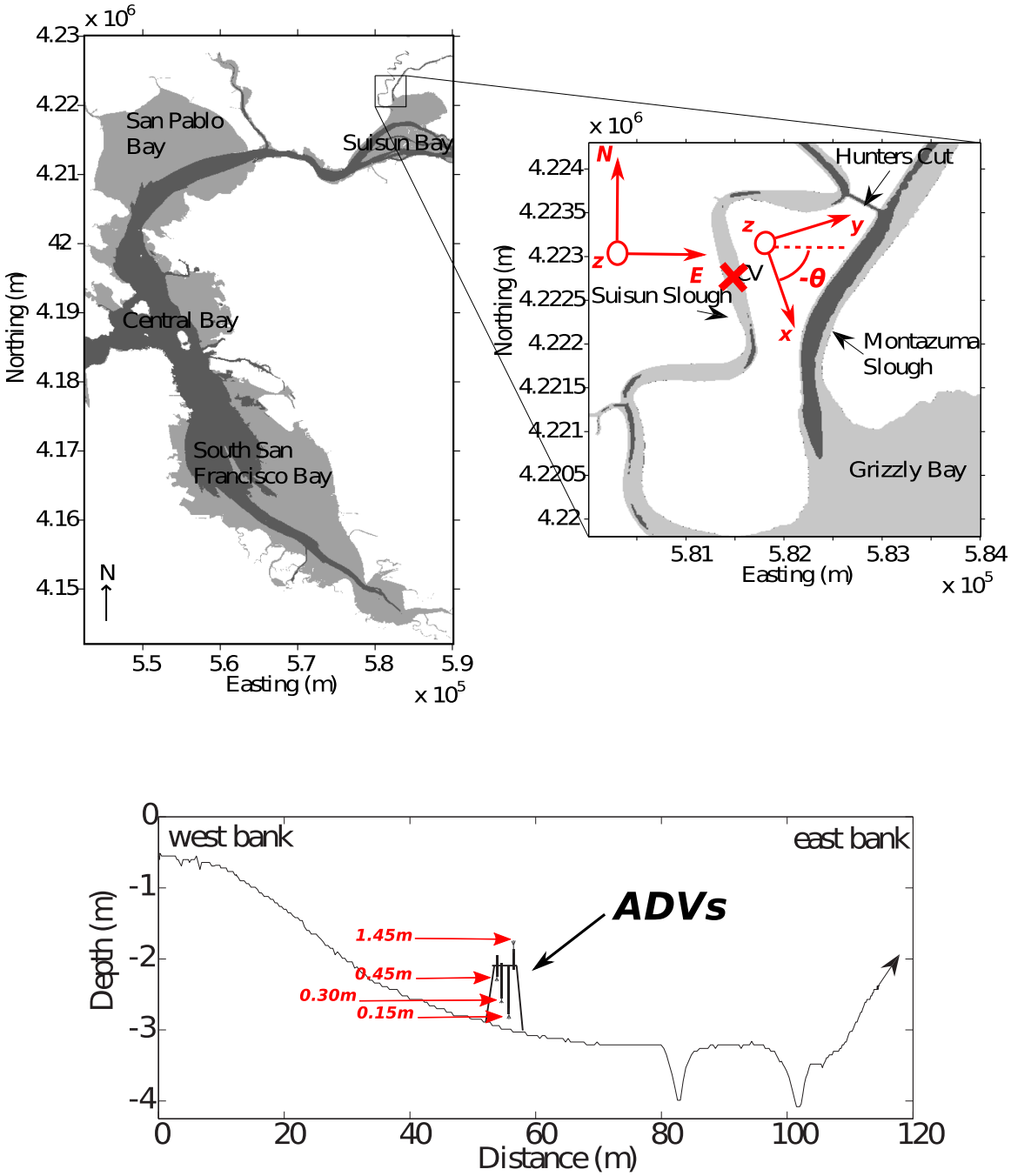

Figure 1. (top) Bathymetric contours and site map of the lower reaches of Suisun Slough. The red cross corresponds to the location of the measurements; the darker gray areas indicate depths greater than 6 m. (bottom) Cross section of the channel where the ADV were situated.

field measurements, which is almost impossible, but rather to demonstrate the successful application of the M13 model.

2. Study Site and Data Set

The data set used here comes from the field experiments of *Jones et al.* [2009] carried out in Suisun Slough in North San Francisco Bay from 30 August to 15 September 2005 (Figure 1). The measurement location was relatively shallow, with the water-depth at the measurement site ranging from 2.5 to 4.0 m with the

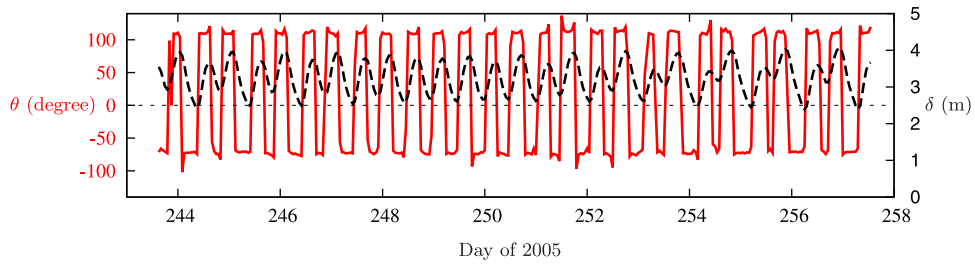

Figure 2. Mean flow direction θ (red solid line) and depth of water (black dashed line) used as boundary layer thickness δ.

semidiurnal tide. Measurements of the three velocity components and pressure were made using Nortek acoustic Doppler velocimeters (ADV) at four different heights, 0.15, 0.30, 0.45, and 1.45 m, above the seabed (ASB). The data set consists of 330 records, or bursts, sampling for 20 min every half hour at 16 Hz. Throughout the remainder of the paper we simply refer to these segments of data as *bursts*. A full description of the experiment and measurement procedure is available in *Jones et al*. [2009].

3. Data Analysis and Selection

3.1. Flow Direction

Each burst of measurements was initially acquired in North, East, and up/down coordinates. The first stage in the data processing is to transpose this system into a right-handed coordinate system in which the streamwise direction corresponds to the mean flow direction (see Figure 1, for the definition of these axis systems). A mean flow angle θ is then determined for each burst, from which the following trigonometry conversion is applied to return the true streamwise and spanwise velocity fluctuations:

$$u = E\cos\theta + N\sin\theta, \tag{2}$$

$$v = N\cos\theta - E\sin\theta. \tag{3}$$

As seen in Figure 2, the site's hydrodynamics are dominated by tidal flow, producing a cyclic change in the mean flow direction and water-depth. The depth of water is calculated as the median value of the pressure sensor data from the four bed-normal locations, and it is used as the boundary layer thickness δ. The tide produces a wide range of flow conditions with a corresponding high variability in Reynolds numbers, as reported in section 3.3.

3.2. Detrending

The natural variability of the tidal channel environment can induce a long-term trend (nonturbulence related), which can interfere with the study of the large-scale turbulent events which are of interest here. Such a trend is clearly visible in the example of the streamwise velocity fluctuations presented in Figure 3a. Filtering out such trends, however, requires caution. The largest-scale motions observed in turbulent boundary layers, or atmospheric surface layers, have been reported to be typically about $10\delta - 15\delta$ in length [*Dennis and Nickels*, 2011a, 2011b, among others]. This is equivalent to 100–150 s in the present data shown in Figure 3a, and appears to be much smaller in duration than the long-term trend. Throughout this paper, the conversion from length to time, and vice versa, is determined the local mean advection velocity. Therefore, we assume that any events longer than 20δ are related to the dynamics of the channel environment, such as long-term trend tidal events which cannot be resolved due to the short sampling length of the bursts, and are not related to the turbulence. The filtering process for separating the long-term trend from the original signal is performed separately for each velocity component and on each burst. We emphasize that this process does not affect the inertial subrange. The velocity signals from the four bed-normal locations are first averaged together. The resulting averaged signal is then low-pass filtered at a cutoff wavelength of 20δ (equivalent to about 200 s) to extract the long-term trend. This trend, shown as a black solid line in Figure 3a, is then subtracted from the raw signals to yield the turbulent fluctuations as illustrated in Figure 3b. Note that for low Reynolds number cases, a spectral gap might exist between the maximal wavelength contained in the bursts and the cutoff wavelength (20δ). In these cases, no trend is

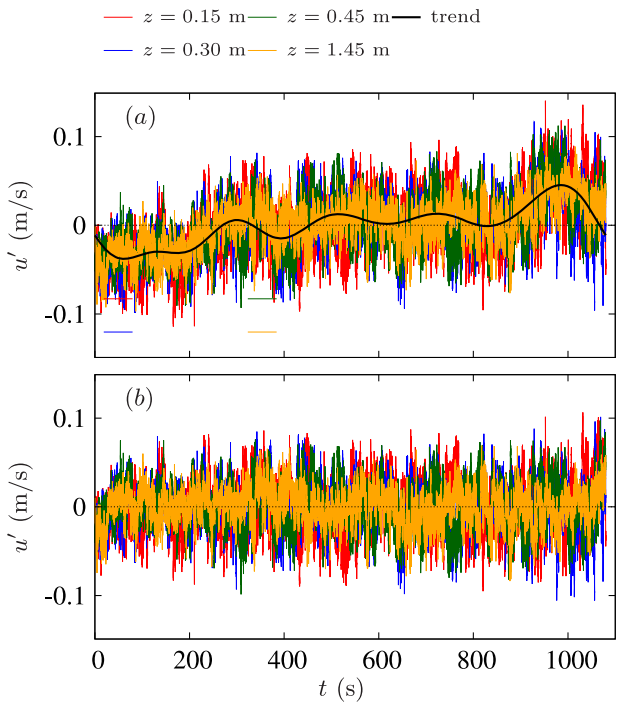

Figure 3. Fluctuating streamwise velocity at each height, (a) before and (b) after detrend. The black solid line in Figure 3a corresponds to the trend calculated by low-pass filtering the average of the four heights. Selected case corresponds to the burst 70, day ∼ 246.5.

removed from the original signal. This circumstance occurs when the tide is changing direction and the current is close to zero. In the following, only the detrended data are considered. The test of stationarity introduced by *Bendat and Piersol* [1986] has been applied for both the mean and standard deviation of the detrended 20 min bursts. It is found that 84% of the bursts pass the test for the mean, and 94% pass the test for the standard deviation.

3.3. Canonical Boundary Layer Properties

The aim of our analysis is to use the wall shear-stress model of *Mathis et al.* [2013] to predict bed information in the tidal channel, and more generally to show its potential for application to environmental flows where accessing such information remains highly challenging. The model was originally developed for a smooth-wall zero-pressure-gradient turbulent boundary layer. It is acknowledged that the model's parameters claimed to be "universal" by M13 for smooth-wall zero-pressure-gradient turbulent boundary layers, might not be fully adequate for the present flow conditions (due to roughness effects, for example). The universality of these parameters remains an open question [*Adrian*, 2010], and while this is beyond the scope of the present study it remains an important consideration for future refinements of the M13 model. If there was variability of these "universal parameters" between different types of wall-bounded flows (e.g., affected by pressure-gradient, roughness, secondary flows, stratification, etc.), this should only affect the accuracy of the model, and not the overall Reynolds number trends [*Mathis et al.*, 2011, 2013].

To adhere to the conditions under which the model was developed, we adopt selection criteria in order to only select the bursts sharing common properties with the canonical turbulent boundary layer. We first need to normalize the whole data set to analyze each burst consistently. This is done by normalizing the raw measurements by the mean friction velocity U_τ for each burst. Unfortunately, direct measurement of the friction velocity in the tidal channel is impossible due to the environmental conditions. Also, the Clauser chart cannot be used due to the limited number of bed-normal data points. Hence, we adopt a different strategy, which consists of estimating U_τ from the Reynolds shear-stress profile, such that $U_\tau = \max\left(\sqrt{-\overline{u'w'}(z)}\right)$. This technique, sometimes referred to as the covariance method [*Kim et al.*, 2000], is often used to predict the mean bed shear-stress [*Kim et al.*, 2000; *Biron et al.*, 2004], and justified in the present case by the fact that the first ADV measurement is very close to the Reynolds shear-stress peak. However, this estimation procedure has limitations [*DeGraaff and Eaton*, 2000], particularly due to the limited vertical range and limited number of measurement points in the bed-normal direction (Figure 4b). Note also that the viscous contribution, $\nu\partial\bar{u}/\partial z$, should be theoretically added to the Reynolds shear-stress in order to strictly respect the bed shear-stress balance. However, the viscous term was neglected since it is lower than 0.15% of the Reynolds shear-stress for the overall database, which is within the measurement uncertainty. Finally, together with the measurement of δ shown in Figure 2, this estimation of U_τ allows us to evaluate the friction Reynolds number. The variation of Re_τ during the whole experimental campaign is presented in Figure 4a. The average Re_τ is around 30,000 but there is a wide range of Reynolds numbers produced by the tidal flow conditions, which provides the opportunity to investigate the Reynolds number dependency of the bed shear-stress fluctuations.

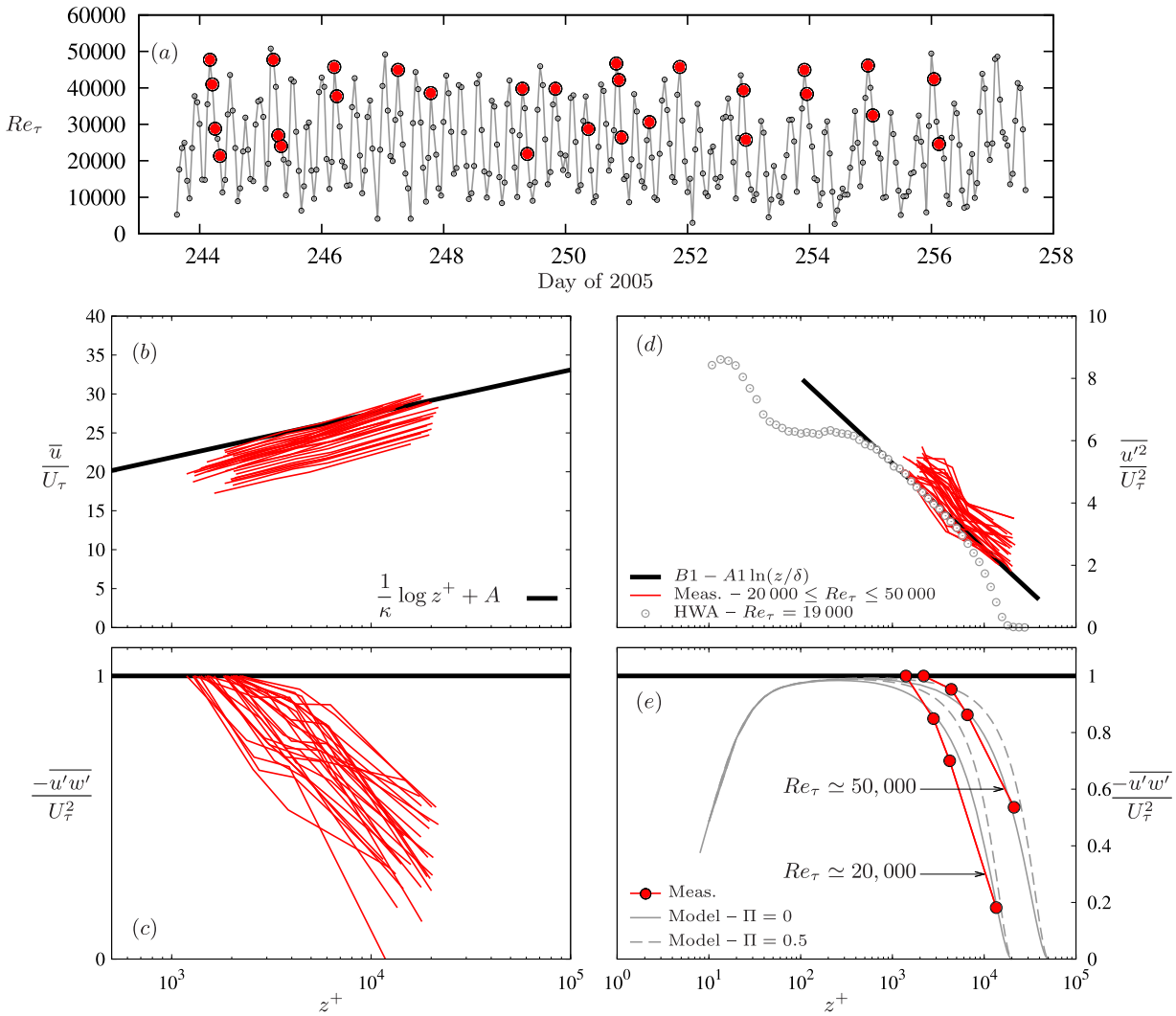

Figure 4. (a) Reynolds number Re_τ of each burst (red dots denote the selected cases); (b) mean velocity profiles, the black solid line shows the log-law of the wall using $\kappa = 0.41$ and $A = 5.0$; (c) Reynolds shear-stress profiles of the selected cases; (d) streamwise turbulence intensity profiles of the selected cases compared to laboratory hot-wire anemometer (HWA) measurements of *Hutchins et al.* [2009] ($Re_\tau = 19{,}000$), the black solid line corresponds to the logarithmic profile with $A_1 = 1.19$ and $B_1 = 1.71$; (e) Comparison of the shear-stress profiles to the model of *Perry et al.* [2002].

To extract the "canonical" segments of data, we then apply the following selection criteria:

1. the vertical profile of the mean streamwise velocity, $\bar{u}$, monotonically increases away from the bed;

2. the vertical profile of the turbulent shear-stress, $-\overline{u'w'}$, monotonically decreases away from the bed;

3. the vertical profile of the streamwise turbulence intensity, $\overline{u'^2}$, monotonically decreases away from the bed;

4. the variability of the points in the mean velocity profile is within 5% of the mean fitted logarithmic-slope (to avoid seesaw trend).

Among these criteria, the first reflects the intrinsic nature of the boundary layer, while the second and third make sense in our experimental configuration since we know that the location of the first off-bed data point is beyond the outer-peak (this will be discussed in section 4). The last criterion ensures that the data do not deviate excessively from a classical log-law behavior of the form $\overline{u^+}_{\text{log-law}} = \frac{1}{\kappa}\ln z^+ + A$. The variability is defined as $\varepsilon_u = \overline{u^+}/\overline{u^+}_{\text{log-law}} - 1$, with $\overline{u^+}_{\text{log-law}}$ a function whose parameters (κ and A) are fitted using only the first three bed-normal locations to ensure that we are safely in the log-region range [see *Marusic et al.*, 2013, for recent discussion about the bounds of the logarithmic region]. It should be emphasized that no

assumption is made about the values of κ and A in the curve fitting. Hence, we only keep the data segments for which the variability is in the range $\varepsilon_u \pm 5\%$. Applying all four selection criteria yields 28 usable cases among the 330 original bursts, covering a range of Reynolds numbers from $Re_\tau \simeq 20,000$ to $50,000$.

Statistics of the selected cases are shown in Figure 4. It should be emphasized that all of these cases have a mean flow direction angle (θ not shown here) between -77 and $-70°$. This corresponds to an ebbing tide. The monotonic behavior is clearly seen in Figures 4b–4d. The mean velocity profiles of the selected segments of data, given in Figure 4b, are consistently below the smooth-wall log-law, as expected for flows with bed roughness. It is worth noting that the mean velocity profiles have the same slope but do not collapse on one another even though they were acquired at the same location. This could indicate a change in the shear-stress balance induced by acceleration terms [*Rowiński et al*., 2000], or more probably a change in the bed roughness, perhaps caused by modifications in the behavior of the benthic community, which includes clams, and/or changing bed forms in the mud. Assuming that the clams are the main contributors to the characteristic roughness height, k, we can anticipate that the boundary layer is sufficiently thick to have a "k-type" roughness $(\delta/k \geq 80)$ [see *Jiménez*, 2004]. As pointed out by *Flack et al*. [2005], this is an important parameter to satisfy the Townsend's Reynolds number similarity hypothesis (a.k.a. "wall similarity"), which states that the turbulence beyond a few roughness heights from the wall is independent of the surface condition. This hypothesis has been verified with rough flows for the turbulent Reynolds stresses and higher order velocity statistics (skewness and kurtosis) [*Flack et al*., 2005], which justifies the application to the present channel measurements even if the bed roughness is not perfectly known. Note in addition that an estimation of the equivalent sand grain roughness [*Nikuradse*, 1933], k_s^+, has been performed over the selected data, and revealed that the flow is likely in a transitionally rough regime $\left(k_s^+ \leq 40\right)$. Assuming a fully rough regime, k_s^+ is related to ΔU^+ through the following relation $k_s^+ = exp[\kappa(\Delta U^+ + 3.4)]$.

For further verification of the canonical behavior of the selected cases, Figure 4e shows a comparison of the Reynolds shear-stress profiles, for the lowest and highest retained Reynolds number cases, against the analytic model of *Perry et al*. [2002]. This model only requires two parameters as input: the Reynolds number and the wake factor Π usually set between 0.4 and 0.6 for a zero-pressure-gradient turbulent boundary layer. For the current comparison, we used two values $\Pi = 0.5$ and $\Pi = 0$. The later corresponds to flow entirely described by the log-law (i.e., no wake). It should be emphasized that the model of *Perry et al*. [2002] should hold for rough walls as well, at least for the log-region and above. This stems from the hypothesis that the wall roughness is only related to the friction velocity U_τ and that the mean relative motions (e.g., velocity differences) and energy containing motions (hence $\overline{u'_i u'_j}$) are not affected by roughness when scaled with this value of U_τ [see *Townsend*, 1976]. Figure 4e shows that the Reynolds shear-stress profiles compare relatively well with the canonical properties (within $\pm 5\%$), even if the peak Reynolds stress cannot be determined accurately due to the small number of points. This indicates that for the high Reynolds number range of the selected cases, the peak Reynolds stress seems to be a reasonable estimate for U_τ. Figure 4e also illustrates that the log-law extends to the maximum measurement height off the bed, with better agreement between the data and the model using $\Pi = 0$, which seems to be the logical assumption for tidal flow. Indeed, the wake parameter should be lower than the value $\Pi \approx 0.5$ usually associated with free-surface of the zero-pressure-gradient boundary layer case, because the tidal channel flow does not guarantee an irrotational flow outside the boundary layer. While reference data of the wake parameter are missing for the present free-surface configuration, it is anticipated that the value of the wake parameter should be closer to a channel flow configuration, $\Pi_{\text{channel}} = 0.05$, in which the flow is fully turbulent at the boundary layer edge.

A final measure of the "canonical" quality of the selected data is obtained by comparing the streamwise turbulence intensity profiles with the laboratory hot-wire anemometer measurements of *Hutchins et al*. [2009] for smooth-wall boundary layer (Figure 4d). The overall trend of the turbulence intensity profiles agrees remarkably well with logarithmic behavior $\overline{u'^2}^+ = B_1 - A_1 \ln(z/\delta)$ [*Marusic and Kunkel*, 2003; *Hultmark*, 2012; *Marusic et al*., 2013]. This result also indicates an extension of the log-layer further above the bed compared with laboratory measurements. This behavior is in accordance with the Reynolds shear-stress profiles, and a flow with a negligible wake component, notably due to the free-surface condition as discussed above.

In summary, Figure 4 shows clear evidence that the retained bursts behave similarly to a canonical turbulent boundary layer, with clear roughness effects being the only significant difference compared to smooth-wall boundary layer flow.

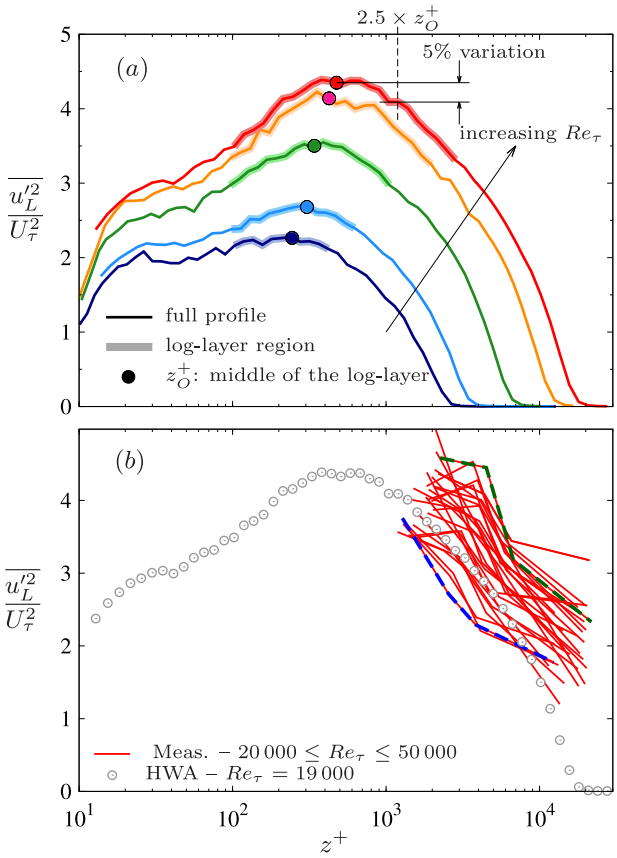

Figure 5. Wall-normal evolution of the large-scale streamwise turbulence intensity $\overline{u_L'^2}^+$ (filter cutoff set to $\lambda_{c,x}$=7000), (a) for laboratory measurements $Re_\tau = 2800$, 3900, 7350, 13,600, and 19,000 [*Hutchins et al.*, 2009; *Mathis et al.*, 2009] (for the highest Reynolds number 5% variation of the peak turbulence intensity occurs at $z^+=2.5\times z_O^+$); (b) for present data compared to the highest laboratory measurement ($Re_\tau = 19{,}000$), the blue and green dashed lines highlight the lowest and highest Reynolds numbers, respectively, $Re_\tau \simeq 21,000$ and $Re_\tau \simeq 48,000$.

4. Construction of the Large-Scale Signal

In the predictive wall shear-stress model developed by M13, (equation (1)), the only input is a large-scale velocity signal. In the original development of the model, this input signal was taken at the logarithmic center of the log-layer, $z_O^+=\sqrt{15Re_\tau}$ [as defined by *Mathis et al.*, 2009]. This choice was motivated by the fact that the middle of the log-region corresponds to the outer-spectral-peak location [see *Mathis et al.*, 2009, Figure 12], as well as to the peak of the large-scale streamwise turbulence intensity profile $\overline{u_L'^2}^+$ [*Mathis et al.*, 2010]. Figure 5a shows an example of the large-scale streamwise turbulence intensity profile obtained in the Melbourne wind tunnel for several Reynolds numbers. In these instances, it is clearly evident that the location where the large-scales are the most energetic agrees very well with the middle of the log-region $z_O^+=\sqrt{15Re_\tau}$. It should be emphasized that the results in Figure 5a are independent of the choice of the cutoff wavelength $\lambda_{c,x}$, which only plays a role in the overall magnitude of the profiles and not on the location of the peak. *Cabrit et al.* [2012] demonstrated that variations in the predicted wall shear-stress might occur if the location of the input large-scale information deviates excessively from the middle of the log-layer. Indeed, any variation from the optimal wall-normal location induces a reduction in the energy of the large-scale signal, as seen in Figure 5a. As the Reynolds number increases, the sensitivity to the wall-normal location is more acute as the peak in Figure 5a becomes sharper.

In the present domain of investigation, i.e., environmental flows, the optimal bed-normal location to capture the necessary large-scale information is not always easily accessible, particularly as U_τ and δ are also subject to variation. Data are usually collected at a fixed bed-normal location. In the present data set, the lowest measurement point ($z = 0.15$ m) is located 2.2–2.5 times above the optimal bed-normal location $z_O^+=\sqrt{15Re_\tau}$. This is visible in Figure 5b, in which the outer-peak of the streamwise turbulence intensity is clearly not captured by the present measurements. However, for the highest laboratory Reynolds number given in Figure 5a, the large-scale turbulence intensity variation in the range $z_O^+ \le z^+ \le 2.5z_O^+$ is less than 5%. Therefore, the following predicted bed shear-stress results should not be significantly influenced by using the measurements from $z = 0.15$ m. The error will be within the measurement uncertainty.

Next, we describe how the input large-scale velocity, $u_{OL}'^+$, is determined using the raw velocity measurement at the first off-bed location (z_1=0.15 m, i.e., $z_1^+ \sim 2.2-2.5\times z_O^+$). Following M13, the raw velocity at z_1^+ is first low-pass filtered at the nondimensional frequency $f^+=2.65\times10^{-3}$ to retain only the large-scale component. Then, the filtered signal is shifted forward in the streamwise direction to account for the large-scale structure angle [see *Mathis et al.*, 2013, for the detailed procedure].

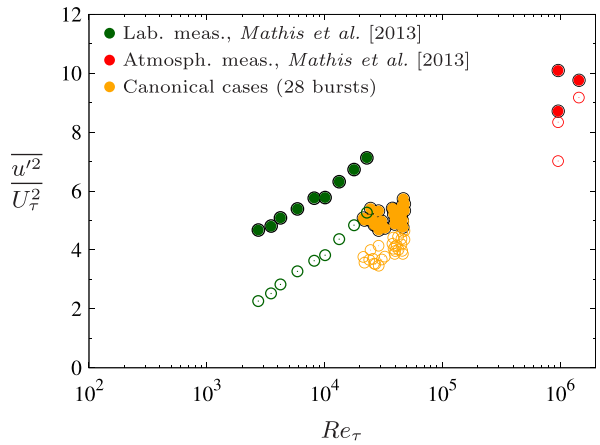

Figure 6. Reynolds number dependency of the streamwise turbulence intensity of the log-region unfiltered signal u'^+_O (filled symbols), and the filtered large-scale component u'^+_{OL} (opened symbols).

In order to assess further the quality of the selected bursts and to support the choice of the first off-bed point, the process is repeated for all bed-normal locations and the corresponding streamwise turbulence intensity is shown in Figure 5b. Only the highest available Reynolds number laboratory measurement is plotted for comparison ($Re_\tau = 19,000$), but one can see that the overall trend is in good agreement.

The Reynolds number trend of the energetic content of the raw and filtered signal for each retained case is shown in Figure 6 for the first off-bed location, along with the laboratory and atmospheric measurements. Overall, both the unfiltered and filtered signals appear to have less energy than the smooth-wall results, but they do follow the same Reynolds number trend. It is unlikely that the lower turbulence intensity of the tidal channel measurements, about 35% lower that laboratory measurements, is directly related to the aforementioned miss-matched optimal bed-normal location (this would only account for around 5% underestimation). This is also evident in the vertical profiles of turbulence intensity, which show that the intensity is much lower for the lowest Reynolds number tidal channel measurement ($Re_\tau \approx 20,000$) compared with the laboratory data (Figure 5b).

Figure 7 shows the spectral content of the outer boundary layer raw streamwise velocity for the present data set and for the laboratory experiment for a similar Reynolds number. The discrepancy between the laboratory and field measurements is more likely due to the changing environment conditions (dynamics of the tidal channel) rather than measurement uncertainties, as differences are seen across all frequencies. However, temporal and spatial resolution issues can also result in a lower turbulence intensity. Indeed, the energy does not approach zero at low wave numbers indicating that the bursts are not long enough to achieve converge of the large-scale content. In addition, the size of the sampling volume of the ADV sensors may be too large to properly capture the smallest scales [*Hutchins et al.*, 2009]. Finally, we emphasize that there is no certainty that the large-scale structures exhibit the same properties in environmental flows, compared to the canonical laboratory configuration.

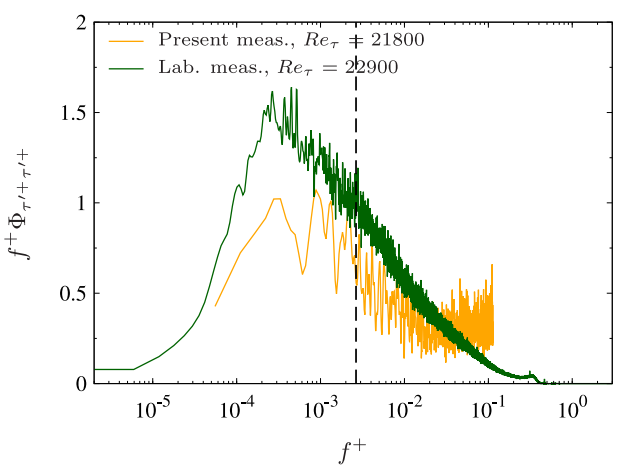

Figure 7. Premultiplied energy spectra of the input streamwise velocity signals for the laboratory [*Mathis et al.*, 2013] and for a single burst of the present measurements (first bed normal point); the vertical dashed line shows the location of the cutoff frequency $f^+ = 2.65 \times 10^{-3}$.

Overall, despite some differences from laboratory measurements in smooth-wall flows, the field measurements selected with simple criteria clearly exhibit the main characteristics of a wall-bounded flow. Note that the main discrepancies occur in the outer-region, where the outer-flow condition may differ from the canonical boundary layer case due to the presence of the free-surface condition in tidal flows. Still, the first off-bed measurements are in the region where the differences remain limited. This strong comparison with the canonical flows, in turn, allows us to apply the bed shear-stress model in the next section, in order to assess its potential and relevance for field measurements.

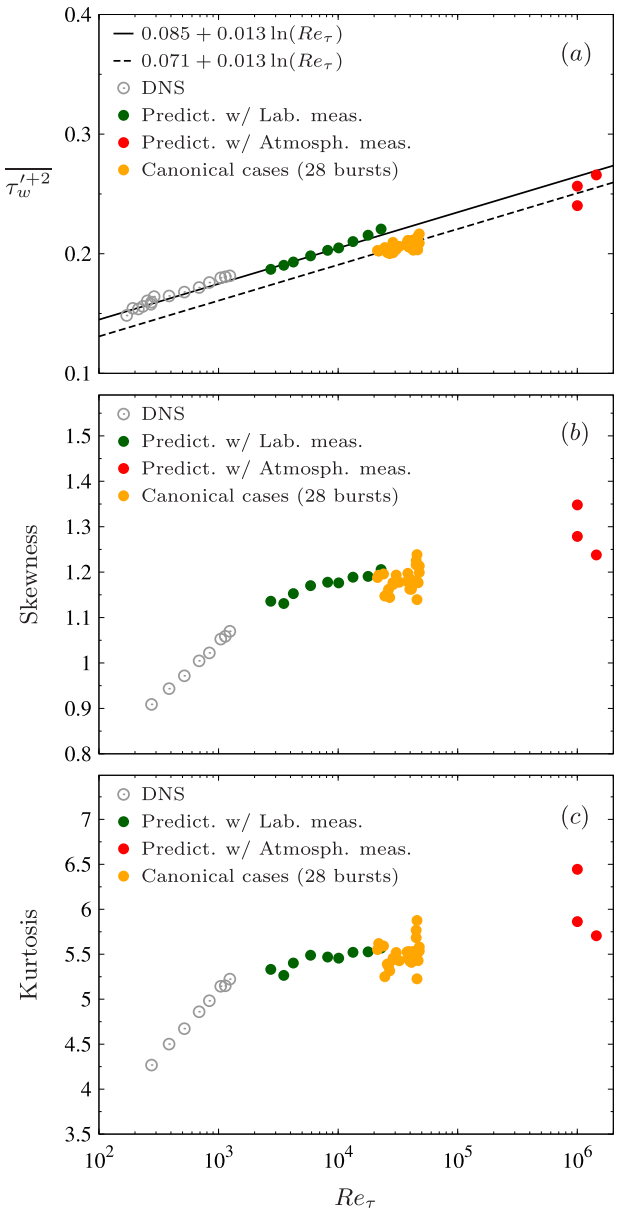

Figure 8. Variance $\overline{\tau_{wp}^{\prime +2}}$, skewness, and kurtosis of the predicted bed shear-stress signal versus the Reynolds number Re_τ, compared to available data for DNS of zero-pressure gradient turbulent boundary layer and former predictions using laboratory measurements.

5. Prediction of the Bed Shear-Stress

5.1. Predictions for the Selected "Canonical" Cases

Below, we present some predictions of the bed shear-stress, $\tau_{wp}^{\prime +}$, using equation (1) and $u_{OL}^{\prime +}$ constituted from the data selected in section 3. The parameter α used in equation (1) comes from a *once-off* calibration measurement at $Re_\tau = 934$, using DNS data set of *del Álamo et al.* [2004] [$\alpha = 0.0989$, see *Mathis et al.*, 2013, for further details]. Figure 8a shows the variance of the reconstructed bed shear-stress signal. Overall, the results agree well with available DNS data and predictions made using laboratory and atmospheric measurements. Note that the wide scatter observed in atmospheric predictions at similar Reynolds numbers is due to the significant measurement uncertainties and difficulties replicating experiments [*Metzger and Klewicki*, 2001; *Kunkel and Marusic*, 2006]. This produces a large variability in the input signal used for the bed shear-stress model, and consequently in the predictions. The Reynolds number trend appears to be correctly captured, and in particular agrees with the atmospheric measurements. However, compared with the laboratory and DNS data a slight underestimation is observed. This is not surprising, considering the aforementioned lower trend of the energy content of the input large-scale streamwise velocity (Figures 6 and 7).

A comparison between the energy content of τ_{wp}^{+} obtained using laboratory and field measurements is given in Figure 9, for predictions made at $Re_\tau \sim 20,000$. Both predictions are very similar with a well captured large-scale content. However, the premultiplied energy for the field experiment is lower than the one of the laboratory experiment at low frequencies which might be responsible for the slight underestimation observed in Figure 8a. For further comparison, higher order statistics are shown in Figures 8b and 8c. We note that the skewness and kurtosis factors of the predicted bed shear-stress signal increase with Reynolds number at a lower rate than the low Reynolds number DNS (Figures 8b and 8c). This is consistent with previous findings and is the subject of ongoing study. Nevertheless, the results seem to agree relatively well with other predictions, even though significant scatter is present, most likely due to the short length of each burst leading to inadequate convergence of the large-scale statistics. Here $TU_\infty/\delta \approx 110$, based on the burst length, $T = 20$ min, and on the mean velocity taken at the furthest measurement point away from the bed, $U_\infty = \bar{U}_{(z=1.45\ \mathrm{m})}$ (which

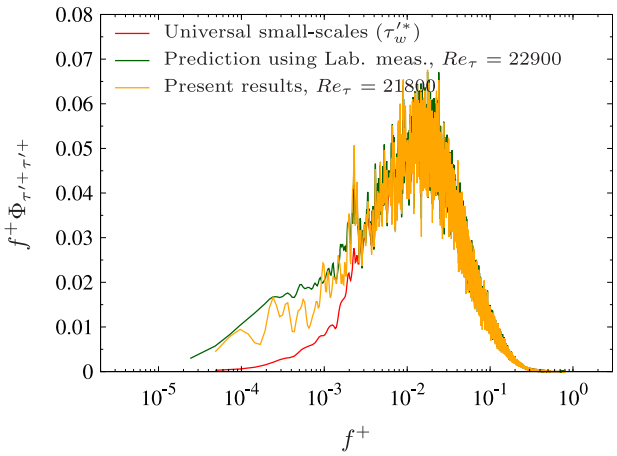

Figure 9. Premultiplied energy spectra of the predicted bed shear-stress signal.

leads to a slight underestimation of TU_∞/δ). It has previously been suggested that this number needs to be large (>5000) for convergence of the large-scale content [*Hutchins et al.*, 2009]. Such an issue is more likely to be encountered in field measurements as a short record length is often required to avoid unsteadiness of the mean flow, e.g., in atmospheric and water-based field measurements. The implications of less than optimal sampling on shear-stress predictions are an important question, especially for higher order statistics, that has been previously addressed by *Sreenivasan et al.* [1978] and *Tennekes and Lumley* [1972]. Another potential source of error stems from the larger than optimal bed-normal location of the large-scale velocity, as discussed previously. However, application of the correction scheme developed by *Cabrit et al.* [2012] to account for the large bed-normal location of the data does not show notable enhancement (not shown). This reinforces our conclusion that the discrepancies observed in Figure 8 are more likely due to the roughness effects of the channel bed rather than measurement uncertainty. We recall that the purpose of our work is not to validate the model for field measurements, but to show its applicability to environmental flows. Our analysis shows that the model predictions for both the laboratory and field observations follow the same trend, indicating the M13 applicability to environmental flows.

5.2. Predictions for the Overall Measurements

We have demonstrated that the field data comply with the characteristics of a canonical turbulent boundary layer and follow similar trends to DNS, laboratory, and atmospheric data. We have applied the model to all of the bursts (330 cases) to determine if data generally comply with the previously observed trends given in Figure 8. The statistical results of the predicted bed shear-stress for all bursts are shown in Figure 10. Despite a noticeable scatter, the overall trend remains similar. Figure 11 shows the probability density function of the residual of the predicted energy intensity, compared to the overall trend of the data as shown in Figure 8a. Integrating this probability density function, we found that around 60% of the overall predictions lay between $\pm$10% of the expected trend. This result confirms the good behavior of the model, even when the input datum does not fully comply with a canonical turbulent boundary layer.

5.3. Instantaneous Predictions

Finally, samples of the reconstructed instantaneous bed shear-stress signal are depicted in Figure 12, along with the outer large-scale streamwise velocity, for the lowest and highest Reynolds numbers cases. Of note are the extended periods of intense positive and negative large-scale streamwise velocities, which are typical of very long large-scale motions (eventually up to 20δ) developing within the log-region [*Hutchins and Marusic*, 2007a]. The amplitude of the bed shear-stress is modulated with variations in the direction of this large-scale streamwise velocity, i.e., the shear-stress is attenuated and amplified for periods of predominantly negative and positive large-scale streamwise velocity, respectively [*Hutchins and Marusic*, 2007b; *Mathis et al.*, 2009]. The highly skewed character of the instantaneous bed shear-stress signal is also obvious. The strong variation of the instantaneous shear-stress raises questions about the efficacy of using conventional mean shear-stress values in sediment transport and ecological modeling. Indeed, the high standard deviation and skewed values of the shear-stress are characteristic of sporadic and violent events, which can drastically influence processes such as nutrient transport across the sediment/water interface and sediment mobilization. Coupling the present predictive model with biogeochemical models could assist the progress of environmental modeling to describe these complex ecological processes.

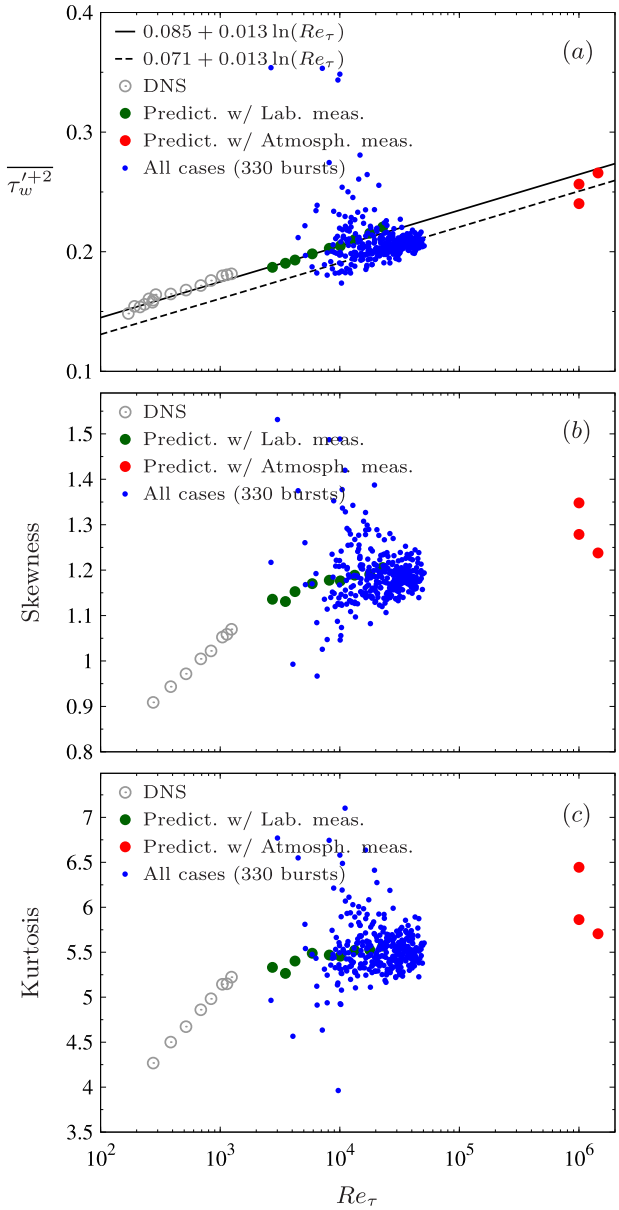

Figure 10. Fluctuation magnitude $\overline{\tau_{wp}'^{+2}}$, skewness, and kurtosis of the predicted bed shear-stress signal versus Reynolds number Re_τ for the whole data set (330 bursts), compared to available data for DNS zero-pressure gradient turbulent boundary layer and former predictions using laboratory measurements. Note that the solid line corresponds to the trend obtained from previous work [*Mathis et al.*, 2013], and the dashed line is reported from Figure 8a.

5.4. Comparison With Conventional Models

In this section, we compare the M13 model with conventional shear-stress models. Two different methods were tested: the log-law and the quadratic stress law. It is important to note that these two conventional methods strictly should not be directly employed for the prediction of the instantaneous bed shear-stress as the underlying physics behind these equations rely on the mean behavior of the flow. However, it is often a common practice to apply them in order to predict the instantaneous large-scale fluctuations, for instance with large eddy simulations [*Piomelli and Balaras*, 2002].

The log-law method corresponds to the equation introduced in section 3.3, in which the mean streamwise velocity is related to the mean shear velocity, U_τ, following a logarithmic relationship:

$$\frac{\bar{u}}{U_\tau} = \frac{1}{\kappa}\ln z^+ + A, \tag{4}$$

where $\kappa = 0.41$ and $A = 5.0$. This method is widely used to find the time-average shear-stress, but suffers from uncertainties when only a few points in z are available to fit the logarithmic profile [*Wilcock*, 1996; *Biron et al.*, 1998], which is the case here. The second method, the quadratic stress law, relates the bed shear-stress to the square of the mean streamwise velocity [*Schlichting and Gersten*, 2000]:

$$\tau_w = \rho C_d \bar{u}^2, \tag{5}$$

where C_d is the drag coefficient, which is usually difficult to estimate accurately [*Dietrich and Whiting*, 1989]. For the present tests, this coefficient was set to $C_d = 0.002$.

To compare the conventional methods to the predictive model proposed in this paper, the closest probe to the bed is used as an input velocity signal, for the burst at $Re_\tau = 21{,}800$. The raw signal is put into each model, which allows us to obtain a predicted instantaneous bed shear-stress signal, τ_{wp}, which is then presented as the bed shear-stress fluctuations scaled in wall units, $\tau_{wp}'^{+} = \tau_{wp}/\overline{\tau_{wp}} - 1$ (note that the uncertainty of the value of C_d is no longer an issue with such a scaling). The premultiplied energy spectra, the probability density function, and samples of the instantaneous predictions are given in Figure 13. As might be expected, the log-law and quadratic stress law models give similar results, but importantly there is almost an order of magnitude difference between the levels of energy spectra compared to the M13 model. It is also interesting to note that the M13 model is the only one able to predict a skewed bed shear-stress.

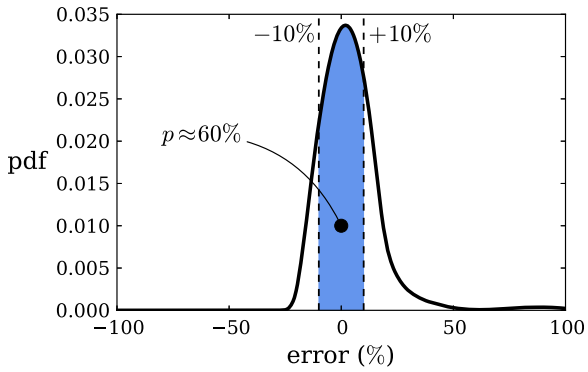

Figure 11. Probability density function of the predicted fluctuating magnitude $\overline{\tau'^{+2}_{wp}}$ of all bursts relative to the overall trend (dashed line) in Figures 8a and 10a. The residual is defined as: residual $=\overline{\tau'^{+2}_{wp}}/[0.071+0.013\ln(Re_\tau)]-1$.

Overall, the strong disparities observed between the conventional models and the present model are not surprising since only the M13 model has been designed to describe the fluctuating component. However, these tests reveal that conventional models must be used with considerable care, and suggest the new approach proposed in this paper should be tested on a wider range of applications.

6. Conclusions

A new wall shear-stress model [*Mathis et al.*, 2013] is considered for environmental applications, where the bed shear-stress is challenging to measure yet crucial for understanding ecosystem dynamics. Here a shallow tidal channel is considered. After applying a set of selection criteria to the data, it is found the tidal channel behaves like a canonical turbulent boundary layer, especially in the logarithmic region. The results show that the lack of near-bed information in field measurements can be overcome by using the predictive model of *Mathis et al.* [2013]. Predictions show a good agreement with the trends from laboratory and DNS results. However, as direct measurements of the instantaneous shear-stress were not available, we note that our analysis does not provide validation of the approach. The relative discrepancies observed in the present case are likely attributed to external conditions, such as roughness effects due to bed forms or benthic organisms. Further work is needed to generalize this approach to account for such additional effects. In particular, two aspects have to be considered. First, due to the dynamic nature of environmental flows such as tidally forced systems, it is difficult to obtain stationary periods of data from which turbulence properties can be extracted. For example, in the present case any sample longer than 20 min will likely be unstationary. Second, environmental flows are subject to variation in bed roughness due to bed forms, benthic organisms and/or canopies, and vertical density stratification can also modify the turbulence [e.g., *Stacey et al.*, 1999; *Perlin et al.*, 2005; *Scully et al.*, 2012; *Bluteau et al.*, 2013]. The effects of these factors have not yet been quantified in the model. We note that the M13 model has several possible routes of improvement which may extend its accuracy and range of applications. For example, the "external" parameters encountered in environmental flows may be incorporated, such as the bed form and vegetation, which could act as dynamical roughness, and also the effects of stratification, unsteadiness, and pressure gradients, to name only a few. The present work has demonstrated the applicability of methods derived from laboratory and DNS flows to directly estimate the instantaneous bed shear-stress in complex and unsteady environmental flows, and its advantages

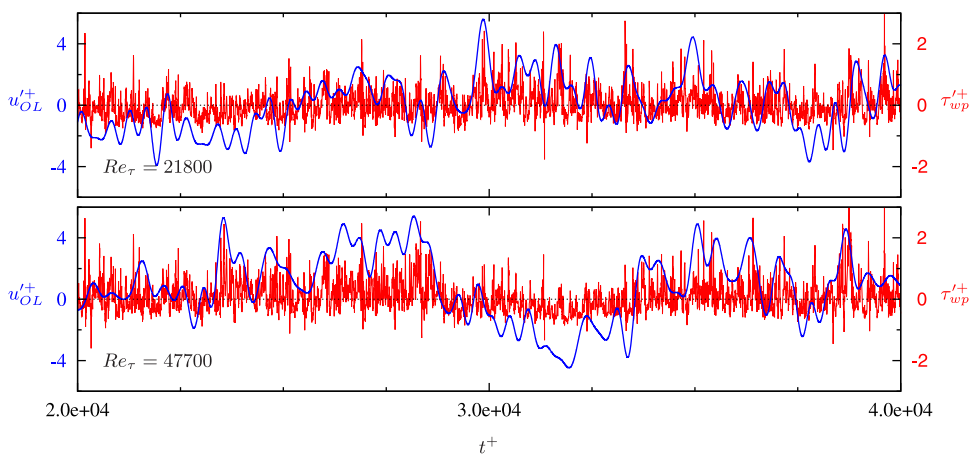

Figure 12. Samples of the predicted instantaneous bed shear-stress signal τ'^+_{wp}, with the input large-scale streamwise velocity u'^+_{OL}. (The dimensional total time-length of the samples is 280 s for $Re_\tau = 21{,}800$, and 90 s for $Re_\tau = 47{,}700$.)

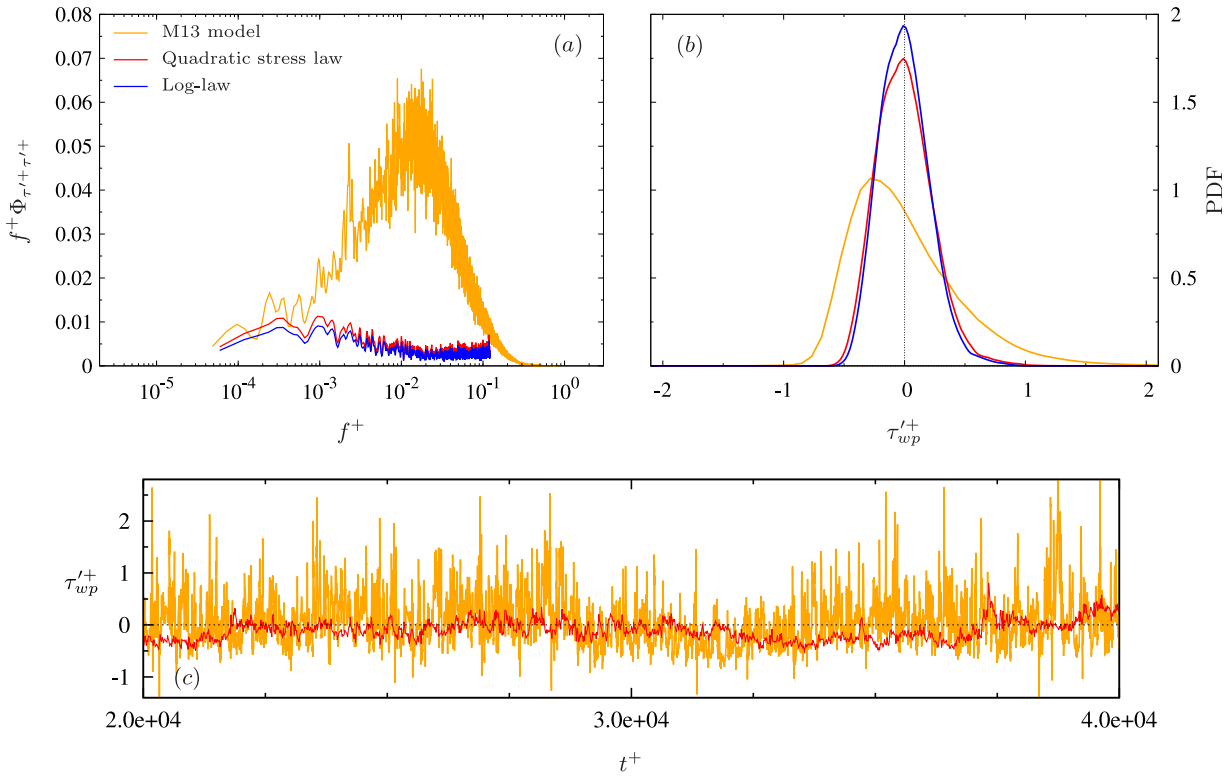

Figure 13. Comparison of the present model against two conventional methods traditionally used to predict the bed shear-stress: the quadratic stress law, and the log-law. The predictions are made using measurements at $Re_\tau = 21{,}800$ as an input signal, and the same color legend is employed in the three subplots: (a) premultiplied energy spectra; (b) probability density function; (c) samples of the predicted instantaneous bed shear-stress signal (note that the fluctuations predicted with the quadratic stress law and the log-law are effectively indistinguishable).

compared to conventional methods. This will ultimately lead to a paradigm shift in the prediction of sediment transport, and the transport of nutrient and contaminants across the sediment-water interface.

Acknowledgments
The Australian Research Council and the University of Melbourne McKenzie Fellowship program are gratefully acknowledged for their support. The field work was supported by the CALFED Bay Delta Authority Restoration Program (ERP02P22) and The Foundation for Young Australians Centenary Scholarship Award. Thanks to F. Parchaso and B. Richards from the U.S. Geological Survey for assistance with the field experiment. The Suisun Slough data set is available from the authors on request.

References

Adrian, R. J. (2010), Closing in on models of wall turbulence, *Science*, *329*(5988), 155–156.
Bandyopadhyay, P. R., and A. K. M. F. Hussain (1984), The coupling between scales in shear flows, *Phys. Fluids*, *27*(9), 2221–2228.
Bendat, J. S., and A. G. Piersol (1986), *Random Data: Analysis and Measurement Procedure*, 2nd ed., Wiley-Interscience, N. Y.
Biron, P. M., S. N. Lane, A. G. Roy, and K. F. Bradbrook (1998), Sensitivity of bed shear stress estimated from vertical velocity profiles: The problem of sampling resolution, *Earth Surf. Processes Landforms*, *23*, 133–139.
Biron, P. M., C. Robson, M. F. Lapointe, and S. J. Gaskin (2004), Comparing different methods of bed shear stress estimates in simple and complex flow fields, *Earth Surf. Processes Landforms*, *29*(11), 1403–1415, doi:10.1002/esp.1111.
Bluteau, C. E., N. L. Jones, and G. N. Ivey (2013), Turbulent mixing efficiency at an energetic ocean site, *J. Geophys. Res. Oceans*, *118*, 4662–4672, doi:10.1002/jgrc.20292.
Cabrit, O., R. Mathis, and I. Marusic (2012), Towards a statistically accurate wall-model for large-eddy simulation, in *18th Australasian Fluid Mechanics Conference*, edited by P. A. Brandner and B. W. Pearce, Australasian Fluid Mechanics Society, Launceston, Australia.
DeGraaff, D. B., and J. K. Eaton (2000), Reynolds number scaling of the flat-plate turbulent boundary layer, *J. Fluid Mech.*, *422*, 319–346.
del Álamo, J. C., and J. Jiménez (2003), Spectra of the very large anisotropic scales in turbulent channels, *Phys. Fluids*, *15*(6), L41–L44, doi: 10.1063/1.1570830.
del Álamo, J. C., J. Jiménez, P. Zandonade, and R. D. Moser (2004), Scaling of the energy spectra of turbulent channels, *J. Fluid Mech.*, *500*, 135–144.
Dennis, D., and T. Nickels (2011a), Experimental measurement of large-scale three-dimensional structures in a turbulent boundary layer. Part 1: Vortex packets, *J. Fluid Mech.*, *673*, 180–217.
Dennis, D., and T. Nickels (2011b), Experimental measurement of large-scale three-dimensional structures in a turbulent boundary layer. Part 2: Long structures, *J. Fluid Mech.*, *673*, 218–244.
Dietrich, W., and P. Whiting (1989), Boundary shear stress and sediment transport in river meanders of sand and gravel, in *River Meandering, Water Resour. Monogr. 12*, edited by S. Ikeda and G. Parker, pp. 1–50, AGU, Washington, D. C.
Diplas, P., C. L. Dancey, A. O. Celik, M. Valyrakis, K. Greer, and T. Akar (2008), The role of impulse on the initiation of particle movement under turbulent flow conditions, *Science*, *322*, 717–720.
Flack, K. A., M. P. Schultz, and T. A. Shapiro (2005), Experimental support for Townsend's Reynolds number similarity hypothesis on rough walls, *Phys. Fluids*, *17*(3), 035102.
Grant, S. B., and I. Marusic (2012), Crossing turbulent boundaries: Interfacial flux in environmental flows, *Environ. Sci. Technol.*, *45*, 1443–1453.

Grant, W. D., and O. S. Madsen (1986), The continental-shelf bottom boundary layer, *Annu. Rev. Fluid Mech.*, *18*, 265–305.
Grinvald, D., and V. Nikora (1988), *Rechnaya turbulentsiya (River Turbulence)* [in Russian], Hydrometeo-lzdat, Leningrad, Russia.
Hultmark, M. (2012), A theory for the streamwise turbulent fluctuations in high Reynolds number pipe flow, *J. Fluid Mech.*, *707*, 575–584, doi:10.1017/jfm.2012.307.
Hutchins, N., and I. Marusic (2007a), Evidence of very long meandering features in the logarithmic region of turbulent boundary layers, *J. Fluid Mech.*, *579*, 1–28, doi:10.1017/S0022112006003946.
Hutchins, N., and I. Marusic (2007b), Large-scale influences in near-wall turbulence, *Philos. Trans. R. Soc. A*, *365*, 647–664, doi:10.1098/rsta.2006.1942.
Hutchins, N., T. Nickels, I. Marusic, and M. S. Chong (2009), Spatial resolution issues in hot-wire anemometry, *J. Fluid Mech.*, *635*, 103–136, doi:10.1017/S0022112009007721.
Jiménez, J. (2004), Turbulent flows over rough walls, *Annu. Rev. Fluid Mech.*, *36*, 173–196.
Jones, N. L., J. K. Thompson, K. R. Arrigo, and S. T. Monismith (2009), Hydrodynamic control of phytoplankton loss to the benthos in an estuarine environment, *Limnol. Oceanogr.*, *54*(3), 952–969.
Kim, K. C., and R. J. Adrian (1999), Very large-scale motion in the outer layer, *Phys. Fluids*, *11*, 417–422.
Kim, S.-C., C. T. Friedrichs, J. P.-Y. Maa, and L. D. Wright (2000), Estimating bottom stress in tidal boundary layer from acoustic Doppler velocimeter data, *J. Hydraul. Eng.*, *126*(6), 399–406, doi:10.1061/(ASCE)0733–9429(2000)126:6(399).
Kunkel, G. J., and I. Marusic (2006), Study of the near-wall-turbulent region of the high-Reynolds-number boundary layer using atmospheric flow, *J. Fluid Mech.*, *548*, 375–402, doi:10.1017/S0022112005007780.
Marusic, I., and G. J. Kunkel (2003), Streamwise turbulence intensity formulation for flat-plate boundary layers, *Phys. Fluids*, *15*, 2461–2464, doi:10.1063/1.1589014.
Marusic, I., R. Mathis, and N. Hutchins (2010), Predictive model for wall-bounded turbulent flow, *Science*, *329*(5988), 193–196, doi:10.1126/science.1188765.
Marusic, I., J. P. Monty, M. Hultmark, and A. J. Smits (2013), On the logarithmic region in wall turbulence, *J. Fluid Mech.*, *716*, R3.
Mathis, R., N. Hutchins, and I. Marusic (2009), Large-scale amplitude modulation of the small-scale structures in turbulent boundary layers, *J. Fluid Mech.*, *628*, 311–337, doi:10.1017/S0022112009006946.
Mathis, R., N. Hutchins, and I. Marusic (2010), Scaling of inner and outer regions for flat plate boundary layers, in *17th Australasian Fluid Mechanics Conference*, edited by Prof. G. D. Mallinson and Dr. J. E. Cater, Faculty of Engineering in association with the Centre for Continuing Education, The University of Auckland, Auckland, N. Z.
Mathis, R., N. Hutchins, and I. Marusic (2011), A predictive inner-outer model for streamwise turbulence statistics in wall-bounded flows, *J. Fluid Mech.*, *681*, 537–566, doi:10.1017/jfm.2011.216.
Mathis, R., I. Marusic, S. I. Chernyshenko, and N. Hutchins (2013), Estimating wall-shear-stress fluctuations given an outer region input, *J. Fluid Mech.*, *715*, 163–180, doi:10.1017/jfm.2012.508.
Metzger, M. M., and J. C. Klewicki (2001), A comparative study of near-wall turbulence in high and low Reynolds number boundary layers, *Phys. Fluids*, *13*, 692–701, doi:10.1063/1.1344894.
Monkewitz, P. A., K. A. Chauhan, and H. M. Nagib (2007), Self-consistent high-Reynolds-number asymptotics for zero-pressure-gradient turbulent boundary layers, *Phys. Fluids*, *19*, 115101–1–115101-12, doi:10.1063/1.2780196.
Nikuradse, J. (1933), Laws of flow in rough pipes, technical report 1292, Natl. Advis. Comm. for Aeronaut., Washington, D. C.
Örlü, R., and P. Schlatter (2011), On the fluctuating wall-shear stress in zero-pressure-gradient turbulent boundary layers, *Phys. Fluids*, *23*, 021704, 1–4.
Perlin, A., J. N. Moum, J. M. Klymak, M. N. Levine, and P. M. Kosro (2005), A modified law-of-the-wall applied to oceanic bottom boundary layers, *J. Geophys. Res.*, *110*, C10S10, doi:10.1029/2004JC002310.
Perry, A. E., I. Marusic, and M. B. Jones (2002), On the streamwise evolution of turbulent boundary layers in arbitrary pressure gradients, *J. Fluid Mech.*, *461*, 61–91.
Piomelli, U., and E. Balaras (2002), Wall-layer models for large-eddy simulation, *Annu. Rev. Fluid Mech.*, *34*, 349–379.
Rowiński, P. M., W. Czernuszenko, and J.-M. Pretre (2000), Time-dependent shear velocities in channel routing, *Hydrol. Sci. J.*, *45*(6), 881–895, doi:10.1080/02626660009492390.
Rowiński, P., J. Aberle, and A. Mazurczyk (2005), Shear velocity estimation in hydraulic research, *Acta Geophys. Pol.*, *53*(4), 567–583.
Schlichting, H., and K. Gersten (2000), *Boundary Layer Theory*, 8th revised and enlarged ed., Springer, Berlin.
Scully, M. E., W. R. Geyer, and J. H. Trowbridge (2012), The influence of stratification and non local turbulent production on estuarine turbulence: An assessment of turbulence closure with field observations, *J. Phys. Oceanogr.*, *41*, 166–185.
Shields, A. (1936), Application of similarity principles and turbulence research to bed-load movement, *Mitt. Preuss. Vers. Wasserbau Schiffbau*, *26*, 5–24.
Simpson, J. H., and J. Sharples (2012), *Introduction to the Physical and Biological Oceanography of the Shelf Seas*, p. 424, Cambridge Univ. Press, N. Y.
Sreenivasan, K., C. J., and R. A. Antonia (1978), Accuracy of moments of velocity and scalar fluctuations in the atmospheric surface layer, *Boundary Layer Meteorol.*, *14*, 341–358.
Stacey, M. T., S. G. Monismith, and J. R. Burau (1999), Measurement of Reynolds stress profiles in unstratified tidal flow, *J. Geophys. Res.*, *104*, 10,933–10,949, doi:10.1029/1998JC900095.
Tennekes, H., and J. L. Lumley (1972), *A First Course in Turbulence*, Mass. Inst. of Technol., Cambridge, Mass.
Townsend, A. A. (1976), *The Structure of Turbulent Shear Flow*, 2nd ed., Cambridge Univ. Press, Cambridge, U. K.
Wilcock, P. R. (1996), Estimating local bed shear stress from velocity observations, *Water Resour. Res.*, *32*, 3361–3366.